Available online at www.sciencedirect.com
ScienceDirect
Journal of the European Ceramic Society 30 (2010) 2917–2925
www.elsevier.com/locate/jeurceramsoc

# Processing and mechanical response of highly textured $Al_2O_3$

Robert J. Pavlacka, Gary L. Messing *

*Department of Materials Science and Engineering, Pennsylvania State University, University Park, PA 16802, United States*

Available online 30 March 2010

**Abstract**

Dense, high quality textured alumina was fabricated by templated grain with only 0.14 wt% ($SiO_2 + CaO$) and 1–15 wt% tabular alumina templates From stereological measurements, texture fraction was 95% and unaffected by template loading or dopant concentration. Due to the excellent template alignment during casting, the full-width at half the maximum (FWHM) of the rocking curve was exceptionally low at 4.6°. Samples with the largest templated grains (1% templated alumina) have much lower strength (300–320 MPa) than those with smaller templated grains (400–500 MPa). Predominantly transgranular crack paths were observed in fracture surfaces both parallel and perpendicular to the oriented grains. The fracture toughness was anisotropic with slightly higher toughness perpendicular to the basal surface than parallel the direction grain basal surface. Surprisingly, the lowest density sample (93%) tested, which started with 15 wt% templates had the highest strength of 511 MPa ± 0.45 and highest fracture toughness of 4.58 ± 0.44 MPa $m^{1/2}$ when measured perpendicular to the basal surface of the grains.


*Keywords:* Texture; Templated grain growth (TGG); $Al_2O_3$; Anisotropy; Fracture

## 1. Introduction

Textured alumina is produced by a variety of processing methods, including high-temperature deformation,[1–3] magnetic alignment of grains during green body formation,[4,5] and templated grain growth (TGG).[6–10] Arguably the highest quality texture in bulk ceramics is achieved by TGG. In TGG processing a subset of template particles is uniformly distributed in a fine powder and the templates are aligned during forming. After densification, the oriented template grains grow preferentially with further heating by consuming the non-oriented matrix grains and, as a result, the final microstructure consists of grains with an orientation distribution that is determined (or templated) by the initial placement and alignment of the template particles.

Templates are aligned during TGG processing of alumina under a doctor blade during tape casting or during uniaxial pressing. For successful TGG processing the template particles are larger than the matrix particles (preferably at least ten times larger) because the size difference is the driving force for preferred growth.[9] The template particles also have a large aspect ratio because most TGG forming processes use shear stresses for template alignment. The larger anisomorphic template particles behave as rigid inclusions and create significant stresses during sintering, and subsequently inhibit densification.[11,12] In the alumina system, previous research showed that by doping with a mixture of CaO and $SiO_2$, and thus creating a calcium aluminosilicate liquid at the grain boundaries during sintering that relaxes the densification-limiting stresses, full densification during TGG processing is enabled.[6]

Beneficial, if contradictory, mechanical behavior is often observed in alumina with microstructural texture. Prior to the advent of the templated grain growth approach, Salem et al. reported toughness increases of 35–40% perpendicular to the *c*-axis and *R*-curve behavior in weakly textured alumina produced by extrusion.[13] Carisey et al. characterized the mechanical properties in gel-cast textured alumina. While they found no significant increase in fracture toughness, they did find a modest 20% increase in flexural strength and a higher Weibull modulus as well as evidence of indentation crack inhibition normal to the *c*-axis.[14] Hall et al. also found no increase in baseline fracture toughness in highly textured alumina fabricated by TGG, though there was evidence of *R*-curve behavior.[15] In addition they observed that, for fracture perpendicular to the *c*-axis, low velocity cracks tend to deflect and propagate intragranularly along the texture-plane. At higher velocities (i.e. popped-in cracks) however, the crack path is transgranular and experiences no deflection.[15] Yoshizawa et al. also observed crack deflection along the texture-plane and reported an extremely high fracture toughness (10 MPa $m^{1/2}$) and strength (>800 MPa) for texture produced by high-temperature deformation of sintered alumina.

* Corresponding author.
*E-mail addresses:* robert.pavlacka@arl.army.mil (R.J. Pavlacka), messing@ems.psu.edu (G.L. Messing).

0955-2219/$ – see front matter © 2010 Published by Elsevier Ltd.
doi:10.1016/j.jeurceramsoc.2010.02.009

These values are suspect, however, because they also reported exceptionally high fracture toughness (up to 7.9 MPa $m^{1/2}$) and strength (up to 790 MPa) for untextured alumina.[16]

Despite the beneficial mechanical response demonstrated in textured alumina, there are no reports in which the microstructure, texture quality, and mechanical properties are correlated. This is, in part, due to both the conflicting results of mechanical testing and the lack of a standard texture quantification technique. The varying results of mechanical testing are partly a result of the difficulty in measuring the fracture properties of highly anisotropic materials. The simplest fracture toughness test, indentation crack measurements, has fallen out of favor and cannot be properly applied to highly textured materials because the crack shape deviates markedly from that assumed in the model.[17] Therefore strength and fracture toughness measurements using standard bend bar specimens is more appropriate. The indentation-strength technique, which involves the creation of controlled flaws of various sizes by Vickers indentation on the tensile surface of fracture mechanics samples, was chosen for this study.[18] Because the crack depth is inferred from the indent load (as opposed to directly measured), this technique provides a measure of 'effective' fracture toughness. Though this differs from results obtained by other conventional fracture mechanics techniques (such as precracked and notched beams), it is potentially more indicative of the true fracture behavior of these materials. An additional benefit of the indentation-strength technique is that it provides a measure of *R*-curve behavior without the need for *in situ* crack observation during testing.

Correlations between texture quality and processing approaches are problematic as a result of the variety of strategies and X-ray techniques used to quantify texture. Basic comparisons of peak heights[19] (or use of the Lotgering factor) fail to describe fundamental aspects of the texture quality such as the orientation distribution or texture fraction. Therefore we quantify the texture quality by fitting rocking curve or pole figure data to an appropriate function (i.e. the March–Dollase function).

Anisotropic shrinkage has been observed in TGG systems due to the presence of the aligned template particles *post* sintering,[20,21] but the dependence of such anisotropy on template loading and dopant content *during* sintering has yet to be explored. In this study we examined microstructure and texture development in alumina with lower dopant concentrations than previously studied to see how lower dopant concentration affects mechanical properties and whether we can improve texture evolution as a result of less matrix coarsening during matrix densification.[6] In this paper we present the sintering behavior, microstructure evolution, texture development, and mechanical properties of the following low-liquid content textured alumina: 0.14 wt% ($CaO + SiO_2$) dopant, and 2 wt% ($CaO + SiO_2$) dopant for template loadings up to 15 wt%. The Si:Ca ratio is maintained at 5:1, so that 0.14% dopant corresponds to 200 ppm CaO and 1000 ppm $SiO_2$.

## 2. Experimental procedure

High purity α-$Al_2O_3$ powder with a particle size of ~200 nm (TM-DAR, purity >99.99%, Taimei Chemical Co. Ltd., Japan) was used for the matrix and single crystal alumina platelets (Advance Nanotechnology Limited, Welshpool, Australia) with a thickness of ~100 nm and a diameter of 3–10 μm were used as templates (Fig. 1). Magnesium nitrate, calcium nitrate, and tetraethylorthosilicate (TEOS) were used as dopant precursors. Menhaden fish oil and 50:50 (wt ratio) ethanol/xylenes were used as the dispersant and solvent systems, respectively. Alumina powder was dispersed in an ethanol/xylenes and fish oil solution and ball-milled for 24 h using high-purity alumina milling media. The appropriate dopant precursor was dissolved in the slurry and precipitated using several drops of dilute $NH_4OH$. Binder and plasticizers (polyvinyl butyral, polyalkylene glycol, and benzyl butyl phthalate) were then added, followed by an additional 24 h milling/mixing step. For templated tapes, the desired amount of alumina templates was ultrasonicated in the solvent and dispersant mixture. This template suspension was added to the slurry in the last 30 min of mixing to limit breakage from milling. Following the mixing step, the slurries were de-aired while stirring until the proper viscosity was reached. The tapes were cast on mylar at 5 mm/s and with a blade height of 376 μm. The dried tapes were cut, stacked, and isostatically laminated at 75 °C and 20 MPa. Binder pyrolysis was performed in air at 0.25 °C/min to 625 °C.

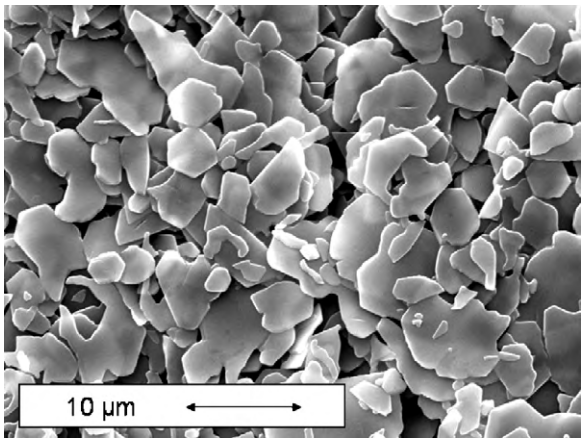


Fig. 1. SEM micrograph of as-received alumina platelets (Advance Nanotechnology Limited, Welshpool, Australia) used as template particles.

Most samples were pressureless sintered in air using a 5 °C/min ramp rate. Cross-sections were polished to a 0.25 μm finish and thermally etched at 100 °C below the sintering temperature to reveal the grain boundaries. Fracture surfaces parallel to the casting direction were obtained to view the basal faces of the templated grains. Samples were gold-coated prior to observation in a scanning electron microscope (SEM) (Philips XL20, Philips Electronic Instruments Co., Mahweh, NJ).

The directional sintering kinetics were observed experimentally by high-temperature dilatometry at 3 °C/min to 1530 °C (the maximum temperature of the apparatus) with a 30 min hold. The total shrinkage was determined by comparing initial and final sample dimensions. Sintered densities were measured using quantitative microscopy (pore counting, >3500 points).

Texture quality was measured using the X-ray rocking curve technique[22] and a standard two-circle X-ray diffractometer with

$CuK_\alpha$ radiation (Scintag, Inc., Cupertino, CA). Two separate scans were collected for each sample. The first scan was a $\theta$–$2\theta$ scan about one of the preferred orientation maxima of the alumina basal orientation, in this case the 000·12 maximum ($2\theta \sim 90.7^\circ$). The second scan was a "rocking scan" using the exact $2\theta$ position obtained in the first scan. With $2\theta$ fixed, the theta scan was collected from $20.35^\circ < \theta < 70.35^\circ$ (or $-25^\circ < \omega < 25^\circ$ where $\omega$ is the angle between the specimen tilt and the texture axis). The data was corrected for defocusing and absorption using TexturePlus.[23] The corrected data is fit analytically to a texture model. For this work we use an axisymmetric texture model; the March–Dollase function[24]:

$$P(f, r, \omega) = f\left(r^2 \cos^2 \omega + \frac{\sin^2 \omega}{r}\right)^{3/2} + (1 - f) \quad (1)$$

Bend bars were machined for strength and indentation-strength testing following the guidelines set by ASTM standard C1161 (with the following exceptions). Samples were sintered into billets approximately 50 mm × 30 mm × 2 mm. One side was polished to a 6 μm finish and the other side was ground until a thickness of 1.5 mm was obtained. Billets were diced into bars and final ground by hand. The edges on the polished (tensile) face were chamfered by grinding with a 1200 grit fixed diamond pad at a 45° angle to mitigate edge cracking. Final bar dimensions were 25 mm × 2 mm × 1.5 mm to within the tolerance set by the ASTM standard. For indentation-strength specimens, the tensile face was indented at loads from 0.5 kgf to 20 kgf using a Vickers indenter. To prevent sub-critical crack growth due to ambient moisture, a drop of silicone oil was placed on each indent and the testing was performed within 24 h of indentation. A semi-articulating SiC 4-point bend apparatus with non-rolling alumina pins, and inner and outer spans of 10 mm and 20 mm, respectively was used. Samples were tested at 0.2 mm/min on a screw-driven Instron universal tester. For each condition, a minimum of 10 bend bars was used for strength testing. A minimum of 3 samples at 4 different indent loads (for a total of 12) was used to obtain fracture toughness from indentation-strength measurements.

## 3. Results

### 3.1. Densification and microstructure development

The axisymmetric (i.e. fiber) nature of the texture (or, conversely, the axisymmetric morphology of grains) results in ∞m symmetry. The unique direction is the normal of the basal (0 0 0 1) surface of the template particles, henceforth called the $z$-direction. The $z$-direction also corresponds to the thickness direction of the individual tapes. The direction perpendicular to the $z$-axis (or parallel to the basal surfaces) is referred to as the $x$–$y$ plane. Therefore, the template particles are aligned within the $x$–$y$ plane.

Fig. 2 shows $x$–$y$ plane shrinkage plotted as a function of temperature for templated alumina with no dopant (Fig. 2a), 0.14 wt% ($CaO + SiO_2$) dopant (Fig. 2b), and 2 wt% ($CaO + SiO_2$) dopant (Fig. 2c), and different template loadings.

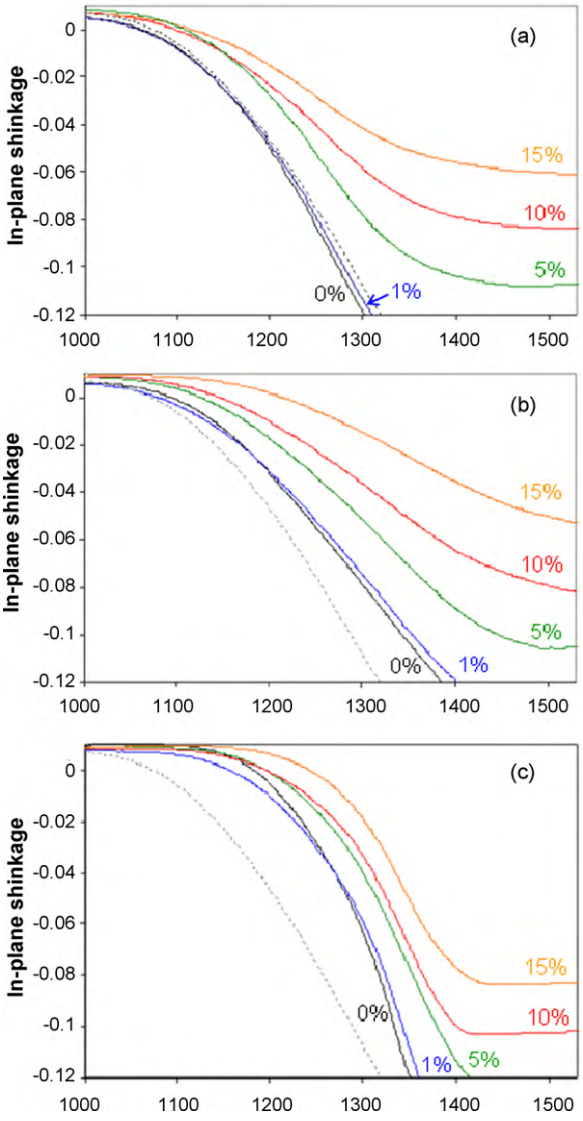


Fig. 2. Shrinkage in the $x$–$y$ plane direction as a function of vol% template loading and temperature during sintering for alumina with (a) no dopant, (b) 0.14% dopant or (c) 2% dopant. Shrinkage was measured by dilatometry during sintering at 3 °C/min to 1530 °C. The dashed line is the shrinkage behavior of non-templated alumina with 1000 ppm MgO.

The (isotropic) densification curve of template-free MgO-doped alumina is included on all plots for comparison. The maximum strain rate ($\dot{\varepsilon}_{max}$), normalized maximum strain rate ($\dot{\varepsilon}^o_{max}$), and temperature at maximum strain rate ($T_{max}$) are plotted in Fig. 3. For samples with a template loading given by $f_{temp}$, the normalized maximum strain is defined as:

$$\dot{\varepsilon}^o_{max}(f_{temp}) = \frac{\dot{\varepsilon}_{max}(f_{temp})}{\dot{\varepsilon}_{max}(0)} \quad (2)$$

where $\dot{\varepsilon}_{max}(f_{temp})$ is the maximum strain rate of the sample and $\dot{\varepsilon}_{max}(0)$ is the maximum strain rate of a template-free sample with the same dopant concentration. Thus, $\dot{\varepsilon}^o_{max}$ is a measure of the relative effect of template loading on $x$–$y$ plane shrinkage for a given dopant concentration.

Total $x$–$y$ plane shrinkage and the instantaneous $x$–$y$ plane strain rate (including $\dot{\varepsilon}_{max}$) are both reduced with increasing

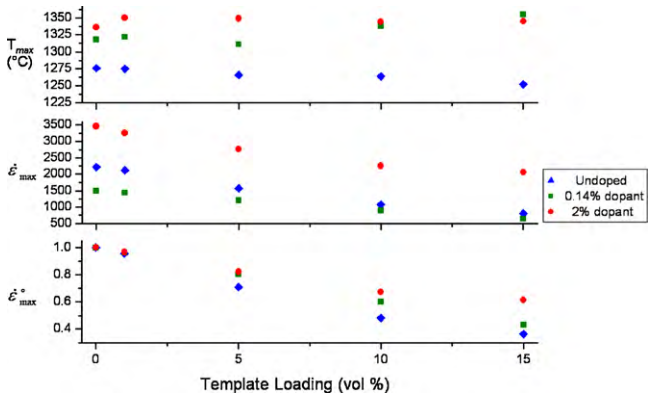


Fig. 3. Shrinkage characteristics extracted from the dilatometry data in Fig. 2, including the temperature at which the strain rate maxima ($T_{max}$), the maximum strain rate ($\dot{\varepsilon}_{max}$), and the normalized maximum strain rate ($\dot{\varepsilon}^{o}_{max}$).

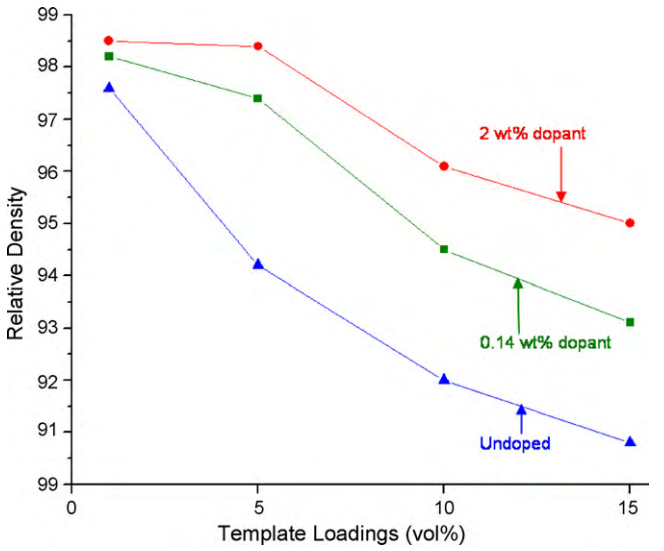


Fig. 4. Sintered density of textured alumina vs. template loading for samples with no dopant, 0.14% dopant, and 2% dopant after sintering at 5 °C/min to 1550 °C with a 90 min hold.

template loading. Template loading, however, has little effect on $T_{max}$. A plot of the instantaneous $x$–$y$ plane strain rate ($d((l - l_o)/l_o)/dt$) vs. time (i.e. the time derivative of Fig. 2) yields a similar result, showing that the templates simply decrease the instantaneous strain rate at all temperatures without changing the shape of the shrinkage curve. Shrinkage in the $x$–$y$ plane for 0 vol% and 1 vol% templated alumina are nearly identical, though $\dot{\varepsilon}_{max}$ decreases by approximately 5%.

As seen in Fig. 3b, there are much higher maximum strain rates in samples with 2 wt% dopant than those with 0.14% or no dopant. In addition, Fig. 2 shows that samples with 2 wt% dopant have greater overall $x$–$y$ plane shrinkage. Greater $x$–$y$ plane shrinkage supports the hypothesis that increasing liquid content provides a mechanism for the relaxation of the stresses associated with constraint imposed by the templates on the matrix (the cause of the reduction in $x$–$y$ plane shrinkage). The introduction of 2% dopant (and 0.14% dopant to a lesser extent) appears to delay the onset of alumina densification as well. This can be seen most clearly in Fig. 2 by comparing the early (or lower temperature) parts of each curve to that of the MgO-doped material. This is also in agreement with Fig. 3a, which shows an increase in $T_{max}$ when the CaO–$SiO_2$ dopant is included.

Interestingly, samples with 0.14% dopant exhibit more gradual $x$–$y$ plane shrinkage (Fig. 2b) and a lower maximum strain rate (Fig. 3b) than undoped samples for all template loadings studied. This is unexpected, since the inclusion of liquid-forming dopants is expected to enhance densification and the concentration of each dopant is above its solid solubility in alumina (and, thus, is expected to form an intergranular liquid phase). It is instructive, however, to consider the effect of dopant concentration on $\dot{\varepsilon}^{o}_{max}$ (Fig. 3c). This shows that $\dot{\varepsilon}^{o}_{max}$ decreases less rapidly with increasing template loading as more dopant is included. Here it is apparent that the $x$–$y$ plane shrinkage of 0.14% dopant samples is less affected by template constraint compared to dopant-free samples, despite the lower absolute strain rates. By this same measure, increasing the dopant concentration to 2% mitigates the effect of template constraint even further.

It is evident from Fig. 2 that several samples are not fully dense at 1530 °C. Preliminary experiments showed that sintered densities approached a maximum for a sintering profile of 5 °C/min to 1550 °C with a 90 min dwell. The effect of dopant concentration and template loading on relative density sintered under these conditions is seen in Fig. 4. Overall densification behavior is clearly inhibited by template constraint, particularly at template loadings greater than 1 vol%. Template constraint has the most pronounced effect on the sintered density of undoped samples, which is the only sample set to exhibit a decrease in density at 1 vol% template loading. There are significant decreases in sintered density of undoped samples at higher template loadings. Samples with 0.14% dopant show improved densification behavior compared to undoped samples. In particular, the effect of template constraint on sintered density is negligible in CaO–$SiO_2$ doped alumina at 1 vol% template loading and minor at 5 vol% template loading. It is only at 10 vol% and 15 vol% template loadings that the consequences of template constraint on density become significant. Samples with 2% dopant exhibit the highest densities for all template loadings. In this case template loadings of up to 5 vol% have very little effect on sintered density.

Macroscopic shrinkage anisotropy was measured for samples sintered at 1550 °C for 90 min. The total $x$–$y$ plane and $z$-direction sintering strain calculated from the initial and final dimensions are plotted in Fig. 5. Increasing template loading decreases $x$–$y$ plane strain and, consequently, increases $z$-direction strain. The much greater $z$-direction strain at a given template loading demonstrates that the templates constrain densification much less than in the $x$–$y$ plane. Dopant concentration has a more significant effect on $x$–$y$ plane shrinkage than $z$-direction shrinkage. While increasing dopant concentration (and thus liquid content) relaxes the template constraint and allows for more $x$–$y$ plane shrinkage, it slightly *reduces* the $z$-direction shrinkage. Alumina with 2% dopant exhibits the least $z$-direction shrinkage despite having higher densities. Because the intergran-

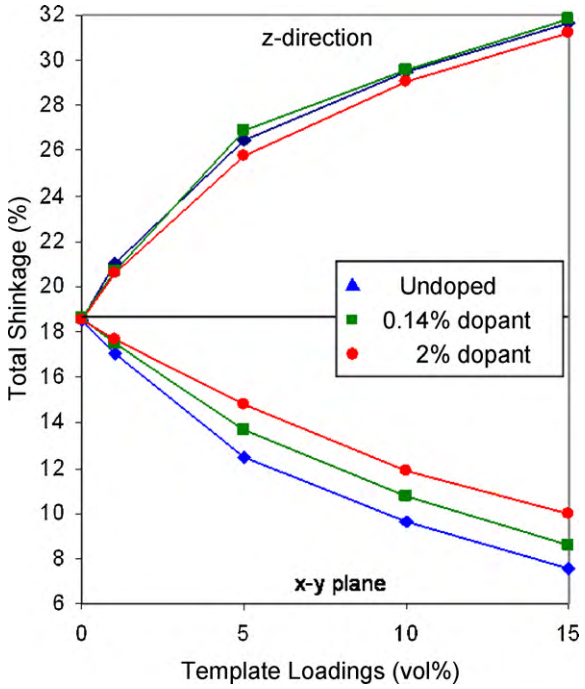


Fig. 5. Total *x–y* plane and *z*-direction shrinkage for samples with no dopant, 0.14% dopant, and 2% dopant after sintering at 5 °C/min to 1550 °C with a 90 min hold.

ular liquid phase improves the densification of TGG materials primarily through improvements in the *x–y* plane shrinkage behavior, it follows that the intergranular phase alleviates some of the template constraint that causes the inhibition of *x–y* plane shrinkage in the first place.

## 4. Microstructure development

The effect of dopant concentration on microstructure development of non-templated alumina is shown in Fig. 6. All samples were sintered at 1550 °C for 90 min. In the absence of $CaO + SiO_2$ dopant, the microstructure remains equiaxed with a grain size of ~4–5 μm. Samples with 0.14% dopant have large, anisomorphic grains, the result of abnormal grain growth. This indicates that this is a sufficient concentration of $(SiO_2 + CaO)$ dopant to create an intergranular liquid phase at the sintering temperature. Samples with 2 wt% dopant are comprised of even larger, anisomorphic grains. The microstructural differences between samples with 0.14% dopant and 2 wt% dopant are the result of changes in temperature at which the intergranular liquid phase appears.[25] Microstructural observations at lower temperatures reveal that abnormal grain growth is initiated at 1450–1550 °C in samples with 0.14% dopant and at <1350 °C in samples with 2% dopant.[25] So, in essence the 2% sample is overfired when sintered at 1550 °C for 90 min. As noted in earlier papers the conditions leading to abnormal grain growth in a ceramic are favorable for TGG since the template particles thermodynamically initiate preferred growth and subsequent grain growth in the desired direction. Furthermore, the template loading regulates the extent of growth to the intertemplate distance in the matrix.

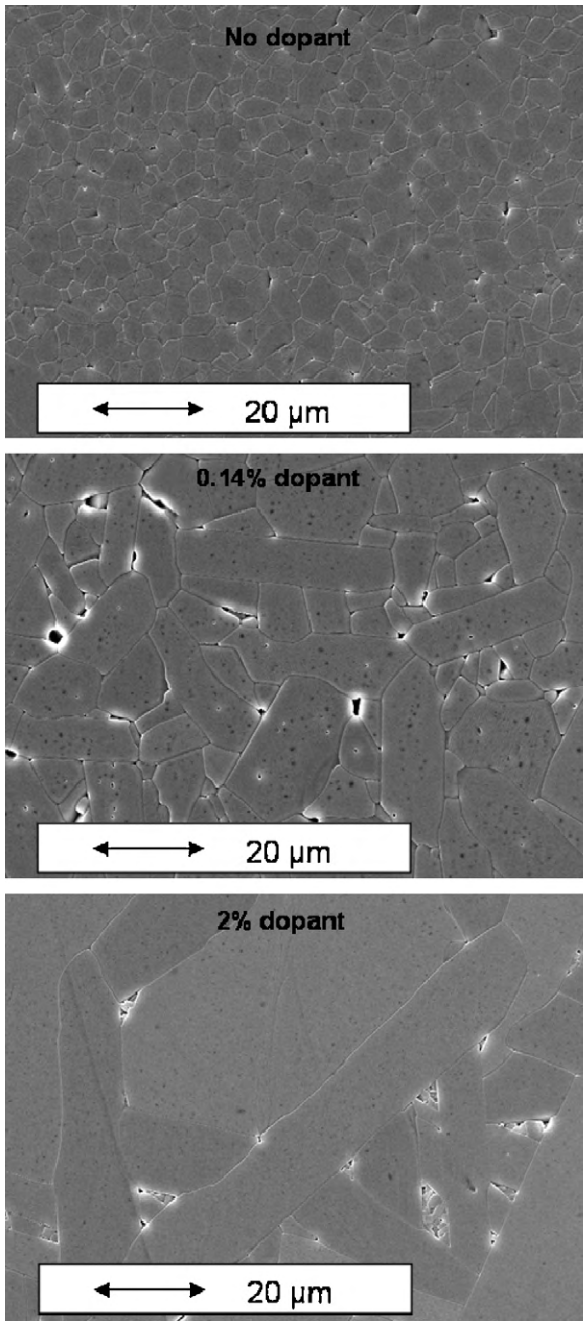


Fig. 6. SEM micrographs showing the microstructures of non-templated $Al_2O_3$ with no dopant (top), 0.14 wt% $(SiO_2 + CaO)$ dopant (middle), and 2 wt% $(SiO_2 + CaO)$ dopant (bottom). All samples were sintered at 1550 °C for 90 min.

The microstructures of the textured aluminas sintered at 1550 °C for 90 min with no dopant, 0.14% dopant, and 2% dopant and two different template loadings (1 vol% and 15 vol%) are shown in Fig. 7. In agreement with Fig. 4, there is an increase in porosity associated with both increasing template loading and decreasing liquid-forming dopant concentration. The porosity is predominately intergranular and is largely situated at the ends of templated grains. The larger pores are a result of *x–y* constraint especially during the sintering before the liquid phase forms (see Fig. 2). The position of the porosity agrees with modeling and observations of Sudre and Lange who showed that a

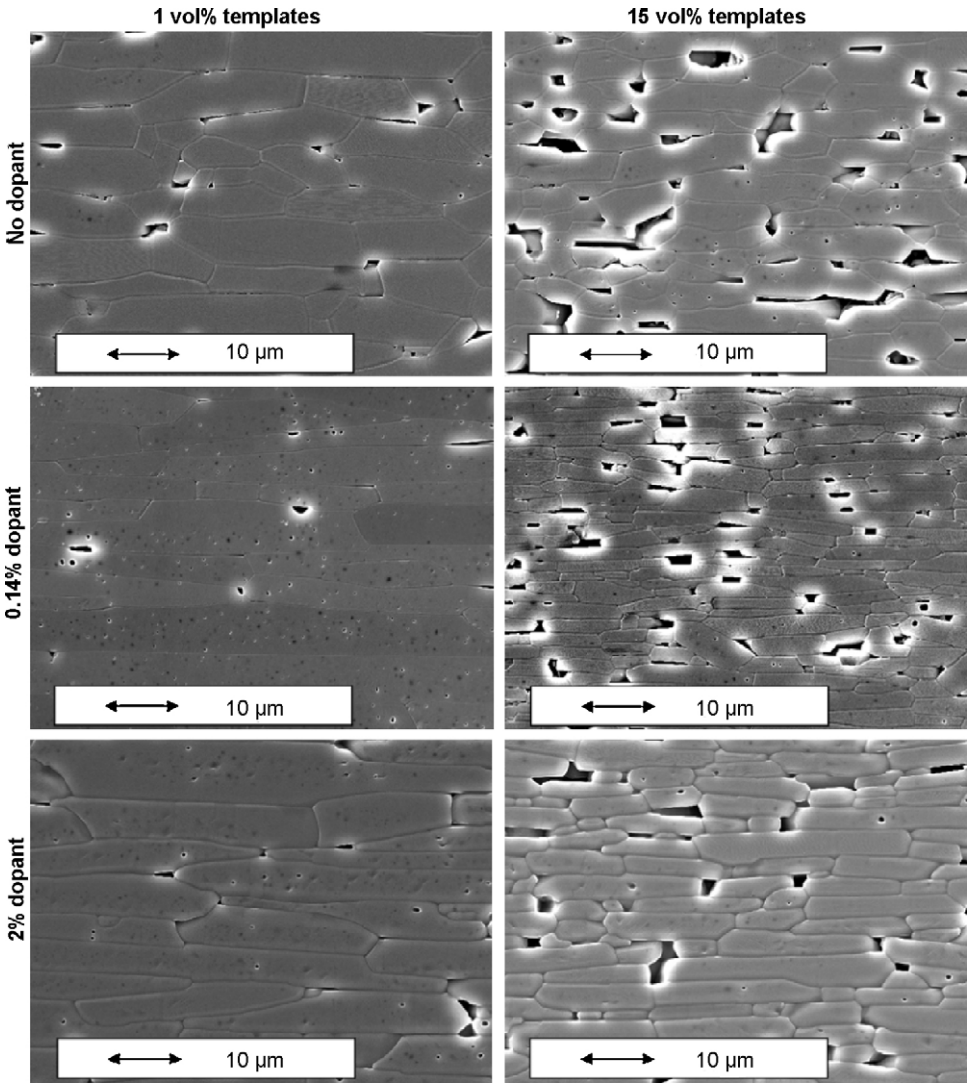


Fig. 7. SEM micrographs showing the microstructures of textured alumina with different ($SiO_2 + CaO$) dopant concentrations and template loadings.

significant tensile stress occurs between the ends of such sharp features.[10,11] In all cases the templated grains grew substantially from the initial template size. However, in samples with no dopant the templated grain aspect ratio is lower and there is a considerable amount of matrix material remaining. The remaining matrix grains have coarsened noticeably and remain during further heat treatment, indicating that they are stable relative to the growing templated grains. In samples with 0.14% and 2% dopant, the microstructure consists of high aspect ratio templated grains and only a few matrix grains. The only macroscopic difference between the samples with 0.14% and 2% dopant is density (Fig. 7).

Finally, it appears that a key to obtaining high density, high texture fraction textured alumina is to maintain a fine matrix grain size during densification below the liquid phase temperature. In the current study, undoped alumina (i) experiences considerable matrix coarsening prior to extensive template growth, reducing the driving force for further template growth, and (ii) does not have liquid phase to relax template constraint. Conversely, previous studies show that texturing in materials with too much liquid phase dopant is limited greatly by matrix coarsening prior to template growth regardless of the ability to relieve template constraint stresses.[26]

## 5. Texture analysis

The effect of template loading and dopant content on texture development was evaluated with rocking curves on the samples shown in Table 1. Texture quality was quantified with $f$ (texture fraction) and $r$ (orientation parameter) by fitting the rocking curves to the March–Dollase equation. The full-width at half the maximum (FWHM) of the rocking curves was also measured, as this is another descriptor of texture quality that has the benefit of being insensitive to the function selection and fitting process. The FWHM measured for 1% templated alumina with 0.14% dopant is exceptionally low (4.6°). A survey of the relevant literature yielded no lower values, indicating that this may be the highest quality axisymmetric texture obtained in a bulk polycrystalline ceramic to date. Fig. 8 shows a $2\theta$ scan of this sample as well as a non-templated (i.e. randomly oriented) but

Table 1
Texture quality including FWHM of the measured rocking curve and calculated March–Dollase parameters.

| Dopant concentration | Template loading | FWHM (°) | $r$ | $f$ (M–D) | $f$ (Ster) |
|---|---|---|---|---|---|
| 0 | 1 | 5.1 | 0.14 | 0.57 | 0.81 |
| 0.14% | 1 | 4.6 | 0.13 | 0.73 | 0.98 |
| 2 | 1 | 5.0 | 0.13 | 0.76 | 0.98 |
| 0.14 | 5 | 6.1 | 0.14 | 0.62 | 0.95 |
| 0 | 10 | 6.9 | 0.17 | 0.63 | 0.86 |
| 0.14 | 10 | 6.2 | 0.16 | 0.66 | 0.98 |
| 2 | 10 | 6.1 | 0.16 | 0.69 | 0.97 |
| 0.14 | 15 | 7.7 | 0.17 | 0.63 | 0.96 |

otherwise identical sample. Note that the intensity axis on the textured alumina plot is broken and that the low intensity section has the same scale as the random alumina plot. The 000·6 and 000·12 maxima, essentially non-existent in randomly oriented alumina, dominate the pattern for the textured sample. The only orientation of significant intensity in the textured material is the 104 peak.

The rocking curve results in Table 1 indicate that the orientation parameter ($r$) increases with increasing template concentration, in agreement with Seabaugh et al.[7] All of the $r$ values in this study are lower than those reported by Seabaugh et al.[7] for all template loadings ($r = 0.185$ for 1 vol% templated alumina). However, direct comparison can be misleading due to the higher aspect ratio templates in our study as well as the different number of template particles for equal template loadings (due to the considerable difference in template sizes). Thus, for equal template loadings by volume, the number of templates in our study is approximately 5 times the number of templates in the work of Seabaugh et al. In addition, the results indicate that texture fraction *decreases*, if modestly, with increasing template concentration. This does not agree with Seabaugh et al., who showed significant increases in texture fraction with increasing template loadings. This can be explained by; (i) the lower number of template particles for a given template loading and (ii) the higher dopant concentration. The first factor increases the growth distances for full texture (i.e. more matrix to consume per template) and the second factors results in greater matrix coarsening prior to and during template growth. The matrix coarsening lowers the driving force for template growth until, for a given temperature, template growth essentially ceases and $f$ is limited.

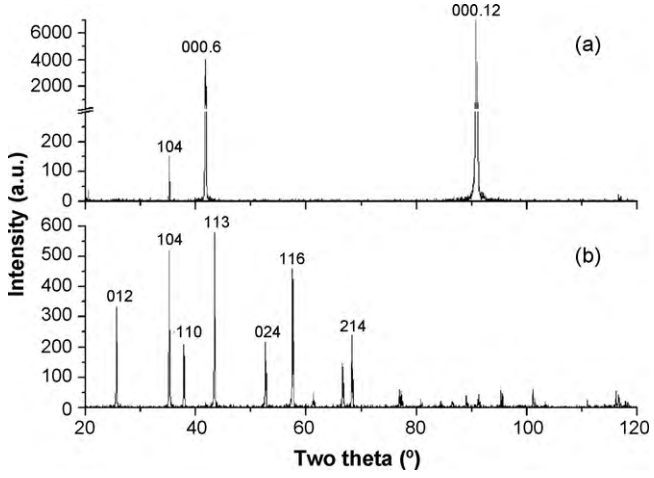


Fig. 8. X-ray diffraction pattern of (a) textured alumina with 0.14% dopant and 1 vol% template loading and (b) non-templated alumina with 0.14% dopant sintered at 5 °C/min to 1550 °C with a 90 min hold.

There is little difference in texture quality for samples with 0.14% and 2% dopant, confirming that 0.14 wt% dopant is sufficient for the production of well-textured, dense alumina. Samples with no dopant, on the other hand, exhibit lower texture fractions, particularly in the case of 1 vol% template loading. This suggests that, template constraint aside, liquid-forming dopants are necessary during TGG for the purpose of encouraging template growth, as observed in Fig. 7. Since we were able to obtain high quality texture with minimal dopant concentration and only a modest decrease in density, the mechanical behavior of the 0.14 wt% doped alumina material was examined.

It should be noted that the $f$ values obtained in the rocking curve analysis may be artificially low due to difficulty in fitting the March–Dollase function to high $\omega$ data (which determines the texture fraction). Therefore, texture fraction was also determined stereologically. Only grains with aspect ratios above 2.5 oriented within 15° of the $x$–$y$ plane were considered part of the texture fraction. Trends similar to those obtained by rocking curve fitting are observed in the stereology results (Table 1), though the overall texture fractions are far higher. Regardless, these results also indicate that a reduction in liquid-forming dopant from 2% to 0.14% does not significantly affect texture quality.

## 6. Strength and fracture behavior

Flexural strength was studied for textured alumina with 0.14% dopant sintered at 1550 °C for 90 min. Testing was performed in two sample orientations having the same fracture plane. The first (parallel) orientation had the tensile surface of the bend bar parallel to the $x$–$y$ plane and the second (perpendicular) is rotated so that the tensile surface of the bend bar is perpendicular to $x$–$y$ plane. Also tested for comparison is a fine-grained equiaxed MgO-doped alumina. The results are given in Table 2. The fine-grained equiaxed $Al_2O_3$ exhibits strength ($507 \pm 45$ MPa) comparable to those reported in the literature for dense fine-grained alumina. Strength in textured alumina, on the other hand, is highly dependent upon the initial template loading and, consequently, the microstructural features. The weakest material tested is the 1% templated alumina ($305 \pm 22$ MPa). Samples with higher template loading are significantly stronger and have statistically similar strengths ($\sim 424 \pm 23$ MPa). Two potential microstructural causes for this change in strength behavior are density and grain size. However the largest differences in sintered density occur between those samples with similar strength values. Moreover, increases in density alone are not commonly associated with *decreasing* strength.[27] It is more likely, and indeed commonly found in equiaxed systems, that strength is reduced with increasing grain size.[28–30] Consider that the final templated grain size (assuming template impingement) is directly determined by the initial template loading and

Table 2
Mechanical properties of textured alumina with 0.14% dopant obtained from 4-point bend testing and indentation strength measurements.

| Sample | Template loading | $\sigma_c$ (MPa) Perp | $\sigma_c$ (MPa) Par | $K_c$ (MPa m$^{1/2}$) Perp | $K_c$ (MPa m$^{1/2}$) Par |
|---|---|---|---|---|---|
| Equiaxed | – | $506 \pm 45$ | | $3.33 \pm 0.14$ | |
| Textured | 1 | $316 \pm 19$ | $305 \pm 22$ | $3.09 \pm 0.35$ | $3.05 \pm 0.23$ |
| Textured | 5 | $421 \pm 38$ | $417 \pm 23$ | $3.93 \pm 0.39$ | $3.03 \pm 0.23$ |
| Textured | 10 | $384 \pm 38$ | $420 \pm 14$ | $3.90 \pm 0.41$ | $3.11 \pm 0.21$ |
| Textured | 15 | $511 \pm 45$ | $436 \pm 32$ | $4.58 \pm 0.44$ | $2.55 \pm 0.31$ |

that the final grain volume is inversely proportional to the number of template particles. As a result, the grain size in the 1% templated sample is significantly larger than the grain size of the higher template loaded samples (see Fig. 7). We should note that it is not just the grain volume that affects the strength but more importantly the large pores created by the greater degree of grain growth. Coarsening of the largest pores will lead to a larger critical flaw size and, thus, a lower strength. Finally, sample orientation does not have a strong effect on flexural strength. This is in agreement with past studies.[13,15]

The effective fracture toughness was determined by the indentation-strength method for the same set of samples. Fine-grained equiaxed alumina was included for comparison. The data for all sample types show excellent agreement with the expected $P^{-1/3}$ dependence of strength ($\sigma_c$), which indicates a single measurable toughness value and no apparent *R*-curve behavior. Effective toughness was calculated from the following expression[18]:

$$K_c = 0.52\left(\frac{E}{H}\right)^{1/8}(\sigma_c P^{1/3})^{3/4} \quad (3)$$

where $K_c$ is the effective fracture toughness, $E$ is the elastic modulus (taken as 393 GPa), $H$ is the hardness of alumina, and $P$ is the indentation load. Attempts to experimentally determine hardness values were thwarted by the tendency for the textured samples to exhibit cracking even at low loads (0.3 kgf). The fracture toughness reported in Table 2 indicates that, in the parallel orientation, there is no increase in toughening due to texturing, in agreement with previous work.[13,14] The effective toughness of 1 vol%, 5 vol%, and 10 vol% templated alumina are similar to each other (3.03–3.11 MPa m$^{1/2}$). The 15% templated samples, however, are much less tough (2.55 MPa m$^{1/2}$). While individual indent crack depths were difficult to determine, a brief post-failure survey of the indents shows no significant dependence of microstructure on crack depth. This suggests that the lower toughness value is actually a characteristic of the 93% dense samples obtained with 15% alumina templates and is not an artifact of the indentation process. In addition, because similar toughness values were obtained for samples with 1 vol% and 5 vol% templates, we conclude that the low strength of 1 vol% templated samples is likely caused by the larger flaw size associated with the increase in grain growth.

Unlike strength, there is a significant effect of orientation on fracture toughness. Higher toughness is observed in the perpendicular direction. This toughness anisotropy is not in agreement with previous studies.[13–15] Moreover, the toughness anisotropy increases with template loading. The fracture surfaces for textured samples tested in both orientations are shown in Fig. 9. Mixed fracture paths (intergranular and transgranular) are observed in both orientations, though transgranular appears to be more dominant in the parallel orientation (Fig. 9b) than in the perpendicular orientation (Fig. 9a). The difference in toughness may be associated with the fracture path and how effectively the differently oriented templated grains can 'bridge' the crack. In the parallel orientation, cracks go through the short dimension (i.e. the thickness) of the templated grains, making them more likely to fail prior to effective bridging. As a result, intergranular fracture is most often observed on just one side of a templated grain (as arrowed in Fig. 9b). In the perpendicular orientation, cracks must go through one of the long dimensions (i.e. the length) of the templated grains. This may make the templated

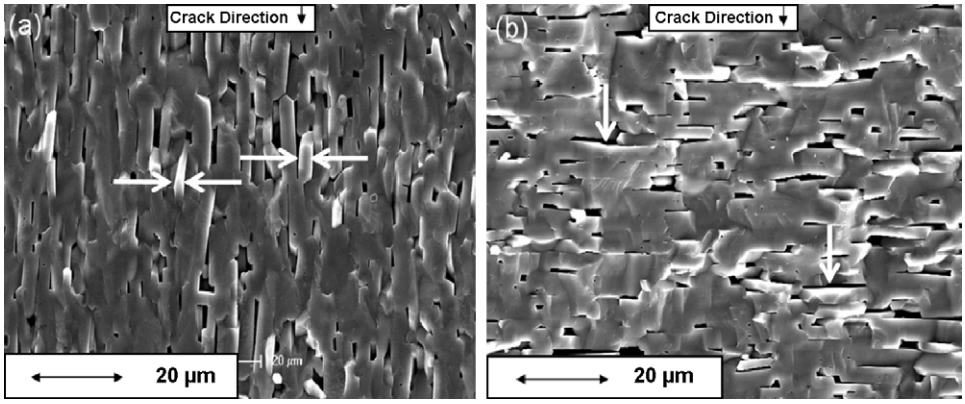


Fig. 9. SEM micrographs showing the fracture surfaces of differently oriented samples following fracture toughness measurement ((a) perpendicular mode and (b) parallel mode).

grains more effective bridges. Instances of intergranular cracking in the perpendicular orientation are commonly observed on both sides of templated grains (as arrowed in Fig. 9a).

Regardless of microstructure and sample orientation all of the observed crack paths are macroscopically straight, traveling in a transverse direction from the indent directly towards the opposite side. This crack morphology is dissimilar from previous examinations of fracture in alumina with strong morphological texture, which show that cracks tend towards parallel with the basal surfaces.[14,15] This is potentially due to a difference in nature of the grain boundaries (i.e. boundary phases and misorientation stresses) between studies, but there is not enough information in the literature from which to draw any conclusions.

## 7. Conclusion

Low-liquid content alumina was textured using the templated grain growth process. In general, liquid-forming dopants delayed the densification process to higher temperatures but allowed for higher densities and improved texture development. *x–y* Plane shrinkage behavior was shown to be very sensitive to the dopant level, particularly in regards to the maximum strain rate.

Extremely high quality texture was achieved, with *r* values as low as 0.13 and FWHM as low as 4.6°. Improvements in texture quality over previous work are, in part, the results of higher aspect ratio templates. It was shown that increasing template loading decreases both the template orientation quality and that 0.14% liquid-forming dopant is a sufficient concentration for obtaining high quality texture.

The flexural strength and fracture toughness of textured alumina with 0.14% dopant and varying template loading were measured in 4-point bend testing. Flexural strength is highly microstructure dependent. Samples with the largest templated grains (1% templated alumina) have much lower strength (300–320 MPa) than those with smaller templated grains (400–500 MPa). Significant fracture toughness anisotropy was observed, with increasing anisotropy accompanying increasing template loading. Predominantly transgranular crack paths were observed in fracture surfaces, which precludes any potential toughening effects from crack bridging.

## References


1. Heuer A, Tighe N, Cannon R. Plastic-deformation of fine-grained alumina ($Al_2O_3$). 2. Basal slip and non-accomodated grain-boundary sliding. *J Am Ceram Soc* 1980;**63**:53–8.
2. Ma Y, Bowman K. Texture in hot-pressed or forged alumina. *J Am Ceram Soc* 1991;**74**:2941–4.
3. Yoshizawa Y, Toriyama M, Kanzaki S. Fabrication of textured alumina by high-temperature deformation. *J Am Ceram Soc* 2001;**84**:1392–4.
4. Suzuki T, Sakka Y, Kitazawa K. Orientation amplification of alumina by colloidal filtration in a strong magnetic field and sintering. *Adv Eng Mater* 2001;**3**(7):490–2.
5. Uchikoshi T, Suzuki T, Okuyama H, Sakka Y. Fabrication of textured alumina by electrophoretic deposition in a strong magnetic field. *J Mater Sci* 2004;**39**:861–5.
6. Seabaugh M, Kerscht I, Messing G. Texture development by templated grain growth in liquid-phase-sintered alpha-alumina. *J Am Ceram Soc* 1997;**80**:1181–8.
7. Seabaugh M, Messing G, Vaudin M. Texture development and microstructure evolution in liquid-phase-sintered alpha-alumina ceramics prepared by templated grain growth. *J Am Ceram Soc* 2000;**83**:3109–16.
8. Carisey T, Laugierwerth A, Brandon D. Control of texture in $Al_2O_3$ by gel-casting. *J Eur Ceram Soc* 1995;**15**:1–8.
9. Suvaci E, Messing G. Critical factors in the templated grain growth of textured reaction-bonded alumina. *J Am Ceram Soc* 2000;**83**:2041–8.
10. Sudre O, Lange F. Effect of inclusions on densification: I, Microstructural development in an $Al_2O_3$ matrix containing a high volume fraction of $ZrO_2$ inclusions. *J Am Ceram Soc* 1992;**75**:519–24.
11. Sudre O, Bao G, Fan B, Lange F, Evans A. Effect of inclusions on densification: II, Numerical model. *J Am Ceram Soc* 1992;**75**:525–31.
12. Salem J, Shannon J, Bradt R. Crack-growth resistance of textured alumina. *J Am Ceram Soc* 1989;**72**:20–7.
13. Carisey T, Levin I, Brandon D. Microstructure and mechanical-properties of textured $Al_2O_3$. *J Eur Ceram Soc* 1995;**15**:283–9.
14. Snel M, van Hoolst J, de Wilde A-M, Mertens M, Snijkers F, Luyten J. Influence of tape cast parameters on texture formation in alumina by templated grain growth. *J Eur Ceram Soc* 2009;**29**:2757–63.
15. Hall P, Swinnea J, Kovar D. Fracture resistance of highly textured alumina. *J Am Ceram Soc* 2001;**84**:1514–20.
16. Yoshizawa Y, Hirao K, Kanzaki S. Mechanical properties of textured alumina made by high-temperature deformation. *J Am Ceram Soc* 2004;**87**:2147–9.
17. Antsis G, Chantikul P, Lawn B, Marshall D. A critical-evaluation of indentation techniques for measuring fracture-toughness. 1. Direct crack measurements. *J Am Ceram Soc* 1981;**64**:533–8.
18. Chantikul P, Antsis G, Lawn B, Marshall D. A critical-evaluation of indentation techniques for measuring fracture-toughness. 2. Strength method. *J Am Ceram Soc* 1981;**64**:539–43.
19. Suzuki T, Uchikoshi T, Sakka Y. Control of texture in alumina by colloidal processing in a strong magnetic field. *Sci Technol Adv Mater* 2006;**7**:356–64.
20. Wei M, Zhi D, Brandon D. Microstructure and texture evolution in gel-cast alpha-alumina/alumina platelet ceramic composites. *Scripta Mater* 2005;**53**:1327–32.
21. Roeder R, Trumble K, Bowman K. Microstructure development in $Al_2O_3$-platelet-reinforced Ce-$ZrO_2$/$Al_2O_3$ composites. *J Am Ceram Soc* 1997;**80**:27–36.
22. Vaudin M, Rupich M, Jowett M, Riley G, Bingert J. A method for crystallographic texture investigations using standard X-ray equipment. *J Mater Res* 1998;**13**:2910–9.
23. Vaudin M. TexturePlus. National Institute of Standards and Technology, Ceramics Division, MD.
24. Dollase W. Correction of intensities for preferred orientation in powder diffractometry—application of the March model. *J Appl Cryst* 1986;**19**:267–72.
25. Pavlacka R. Processing and mechanical behavior of $Al_2O_3$ microstructure composites. PhD thesis. Pennsylvania State University, State College, PA; 2009.
26. Seabaugh M. Texture development in liquid phase sintered alpha alumina via anisotropic template growth. PhD thesis. Pennsylvania State University, State College, PA; 1998.
27. Knudsen F. Dependence of mechanical strength of brittle polycrystalline specimens on porosity and grain size. *J Am Ceram Soc* 1959;**42**:376–87.
28. Spriggs R, Vasilos T. Effect of grain size on transverse bend strength of alumina and magnesia. *J Am Ceram Soc* 1963;**46**:224–8.
29. Passmore E, Spriggs R, Vasilos T. Strength-grain size-porosity relations in alumina. *J Am Ceram Soc* 1965;**48**:1-&.
30. Bennison S, Chantikul P. Role of grain-size in the strength and R-curve properties of alumina. *J Am Ceram Soc* 1990;**73**:2419–27.